Understanding DABCO Nanorotor Dynamics in Isostructural Metal-Organic Frameworks

Supporting Information

Nicholas C. Burtch,[†] Ariana Torres,[‡] Guo Shiou Foo,[†] Johannes Leisen,[§] Carsten Sievers,[†] Bernd Ensing,[‡] David Dubbeldam,[‡] Krista S. Walton[†,*]

†School of Chemical and Biomolecular Engineering, Georgia Institute of Technology, Atlanta, Georgia, United States

‡Van't Hoff Institute for Molecular Sciences, University of Amsterdam, Amsterdam, The Netherlands

§School of Chemistry and Biochemistry, Georgia Institute of Technology, Atlanta, Georgia 30332, United States

Table of Contents

Experimental Section

The Zn-DMOF and Zn-DMOF-TM samples were synthesized and activated according to the procedures described in reference 1. The ligand used in the synthesis of the Zn-DMOF-TM structure containing deuterated DABCO (98.4% ^{2}H) was purchased from C/D/N Isotopes Inc.

Powder X-Ray Diffraction Patterns

Powder X-ray diffraction patterns were obtained using an X'Pert X-ray PANalytical diffractometer with an X'accelerator module using Cu Kα (λ = 1.5418 Å) radiation at room temperature and a step size of 0.02° in two theta. The Zn-DMOF powder XRD pattern was collected in DMF solvent in order to prevent structural breakdown caused by ambient air exposure and this, combined with particle size effects, can have an affect on peak broadness and intensity relative to the simulated single crystal pattern.

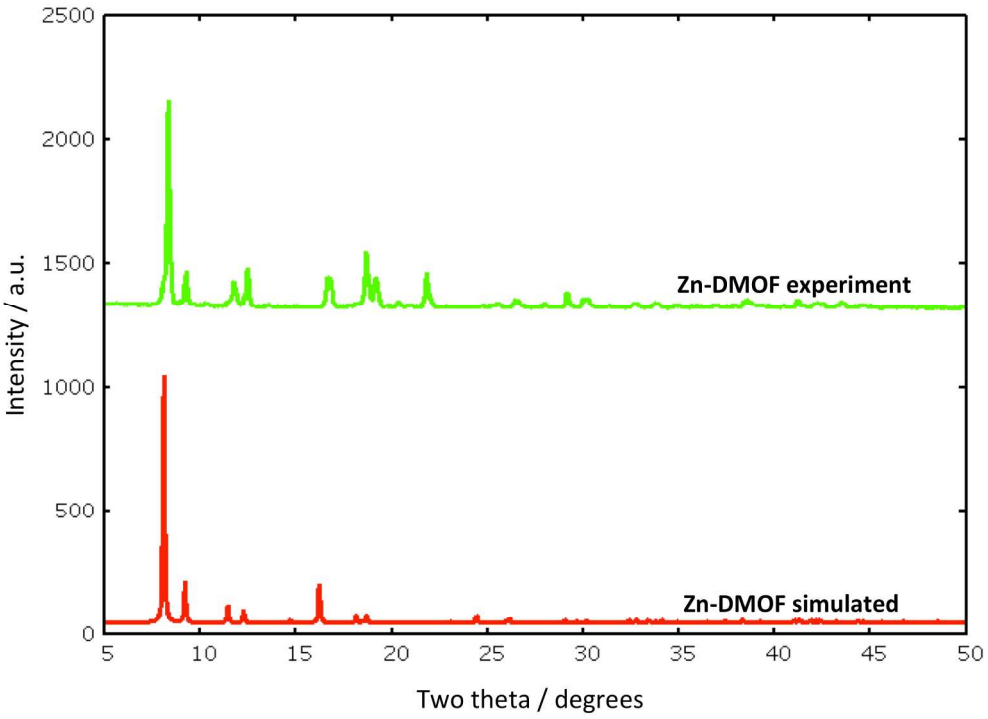

Figure S1: Powder X-Ray diffraction patterns for the as-synthesized Zn-DMOF structure obtained from experiment (green) and the theoretical Zn-DMOF pattern generated based on single crystal data (red).

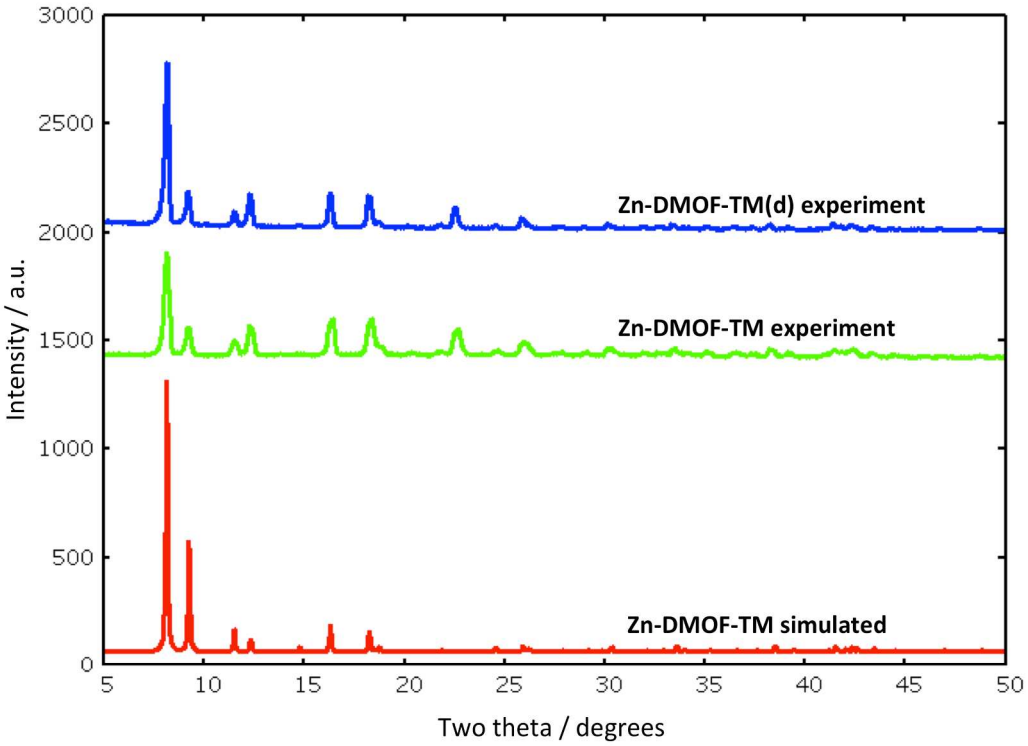

Figure S2: Powder X-Ray diffraction patterns for the as-synthesized Zn-DMOF-TM(d) structure containing the deuterated DABCO ligand (blue), Zn-DMOF-TM with the non-deuterated DABCO ligand (green), and the theoretical Zn-DMOF-TM pattern generated based on single crystal data (red).

BET Analysis via N_2 Adsorption at 77 K

N_2 adsorption at 77 K was performed after sample activation using a Quadrasorb system (Quantachrome Instruments). Experimental BET surface area values were derived from the experimental isotherms using appropriate consistency criteria[2] and are 1020, 1050, and 2040 m^2/g for Zn-DMOF-TM(d) containing the deuterated DABCO ligand, Zn-DMOF-TM with the non-deuterated DABCO ligand, and Zn-DMOF, respectively. These values are in agreement with the theoretical geometric surface areas[3] for the structures as probed by N_2 which range from 1040-1430 m^2/g for the Zn-DMOF-TM structure and 1660-2090 m^2/g for the Zn-DMOF structure (depending on whether a σ or $2^{1/6}$σ Lennard-Jones overlap criterion is used for the N_2 probe molecule).

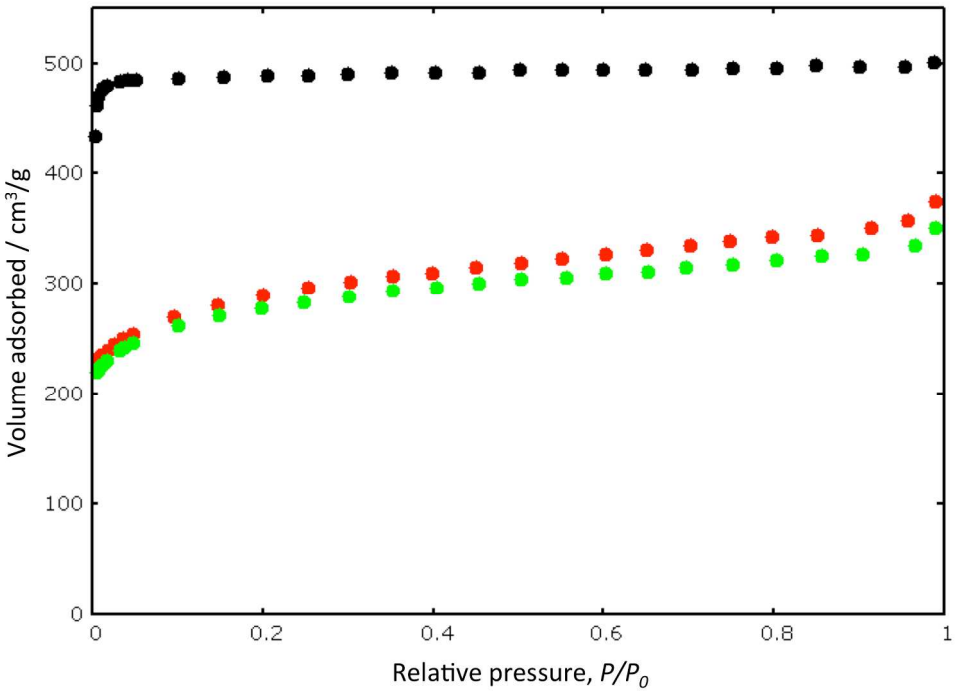

Figure S3: N_2 adsorption isotherms measured at 77 K for Zn-DMOF (black), Zn-DMOF-TM with the non-deuterated DABCO ligand (red), and Zn-DMOF-TM(d) containing the deuterated DABCO ligand (green).

Solid-State NMR

^{1}H - ^{13}C WISE

Using a glove box, activated MOF samples were loaded directly into the ZrO_2 4 mm magic-angle spinning (MAS) rotor which was then sealed using Kel-F caps and kept in air-tight containers until the time of measurement. A Bruker DSX-300 NMR spectrometer was then used in combination with a dual channel MAS probe to measure the ^{1}H - ^{13}C wideline separation (WISE) experiments.[4] Radio frequencies of 75 and 300 MHz were used for ^{13}C and ^{1}H, respectively. The WISE experiment correlates dynamic information as detected by the width of the ^{1}H line-shapes with structural information detected via the ^{13}C chemical shift. The width of the ^{1}H lineshapes is given by the homonuclear dipolar coupling between ^{1}H atoms. MAS will scale this coupling so it is important to conduct the WISE experiment at low spinning frequencies. The WISE spectra were therefore recorded at a spinning frequency of 3 kHz. Spinning sidebands in the ^{13}C dimension were suppressed using the TOSS (total suppression of spinning side bands) technique.[5] Unfortunately, this technique sometimes leads to spectra that cannot be perfectly phased. A short contact time of 0.5 ms was used in order to avoid spin-diffusion between individual sites. A total of 256 scans were accumulated for each individual slice and a recycle delay of 4 seconds between scans was used. The increment in the t_1 dimension was 5 microseconds. Processing the WISE spectrum by a two dimensional Fourier transformation might preclude minor details between the ^{1}H lineshapes associated with individual ^{13}C sites. This is not the case if data are only transformed in the ^{13}C dimension. This leaves a relaxation function for the ^{1}H dimension allowing the very accurate comparison of data in the ^{1}H dimension.

^{13}C NMR

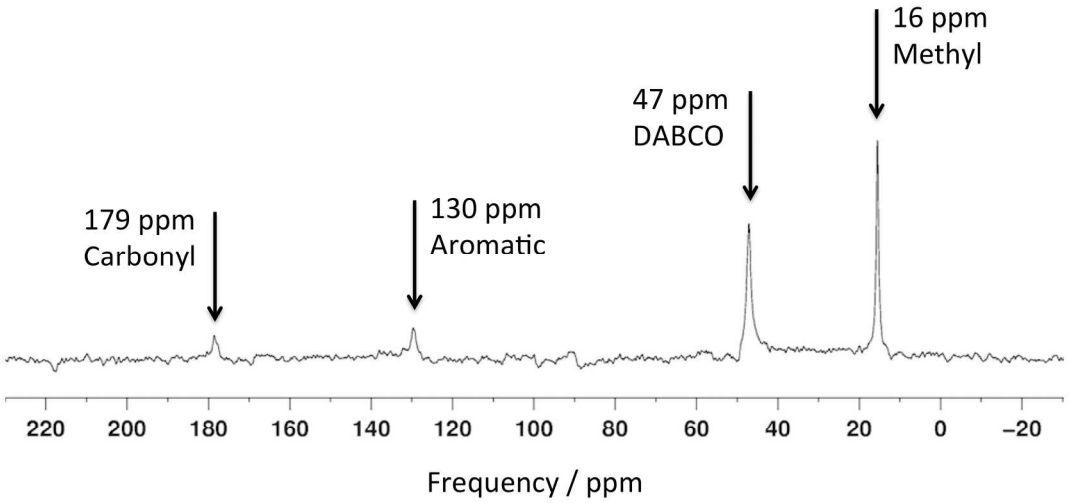

Figure S4: Solid-state ^{13}C CP-MAS NMR spectrum for Zn-DMOF-TM. The data were measured at conditions comparable to the WISE experiment (slow spinning speed of 3 kHz to retain the ^{1}H-dipolar coupling and associated ^{1}H lineshapes, short contact time of 0.5 ms to avoid spin-diffusion, TOSS sequence to partially suppress spinning side-bands).

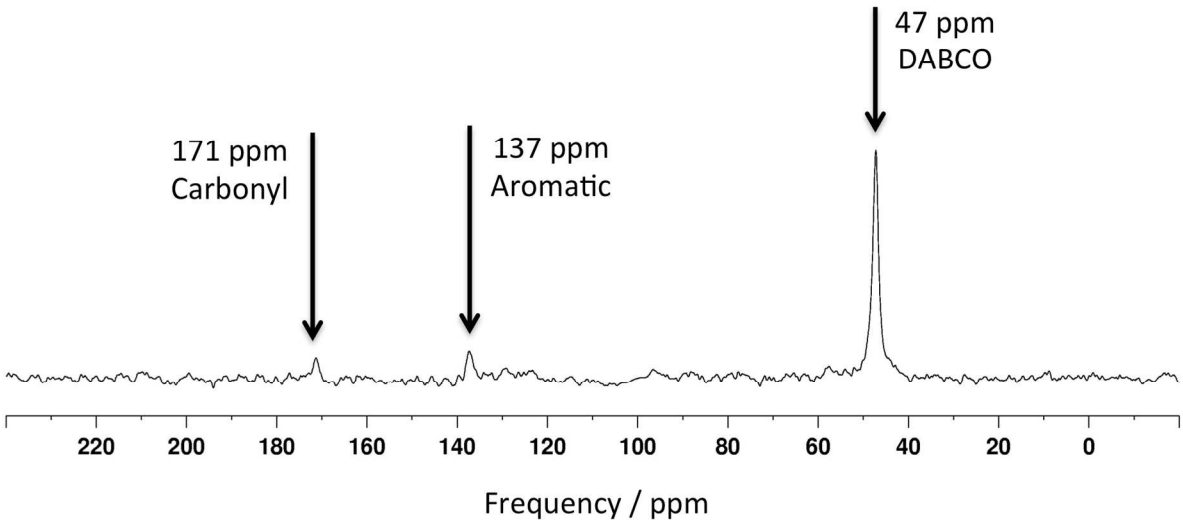

Figure S5: solid-state ^{13}C CP-MAS NMR spectrum for Zn-DMOF. The data were measured at conditions comparable to the WISE experiment (slow spinning speed of 3 kHz to retain the ^{1}H-dipolar coupling and associated ^{1}H lineshapes, short contact time of 0.5 ms to avoid spin-diffusion, TOSS sequence to partially suppress spinning side-bands, data were processed to suppress a common artifact at the excitation frequency).

^{2}H NMR

^{2}H NMR experiments were conducted using a Bruker DSX300 NMR spectrometer with a static probe and exchangeable coil-inserts allowing wideline experiments at different frequencies. Experiments were conducted at 46.08 MHz using the quadrupolar echo sequence[6] consisting of two $\pi/2$ pulses separated by a delay of 30 μs. For each spectrum at least 512 scans were recorded using a relaxation delay of 2 seconds.

FTIR Spectroscopy

Spectra were collected on a Nicolet 8700 FTIR spectrometer with a MCT/A detector. For each spectrum, 64 scans were recorded at a resolution of 4 cm^{-1}. A small amount of Zn-DMOF-TM (2 mg) was spread and pressed on top of a KBr disk. The sample was loaded into a FTIR transmission vacuum chamber and activated at 110 °C under a high vacuum for 12 h. The sample was cooled down to room temperature and a spectra were collected. Various pressures of D_2O vapor was then introduced into the chamber and equilibrated for 45 min. It was noted by Tan et al.[7] that using D_2O instead of H_2O is preferred because it avoids interference between the infrared absorption bands of trace amounts of unreacted H_2BDC molecules and H_2O. This same decision was made in this work, and therefore also allows a direct comparison to the mode assignments in the difference spectra obtained by Tan et al. Subsequently, the chamber was evacuated for 2 h and another spectrum was collected. The sample was re-activated at 110 °C for 12 h, cooled down to room temperature, and a spectrum was collected again.

When various pressures of D_2O vapor are in contact with Zn-DMOF-TM, the FTIR absorption spectrum is strongly affected. A band at 1720 cm^{-1} appeared when the sample was exposed to 0.2 mbar of D_2O vapor and it is assigned as the νC=O vibrational mode.[7] As the pressure increased from 0.2 mbar to 13 mbar, this band red shifted to 1712 cm^{-1}, suggesting that the C=O bond is deuterium bonded to the incoming D_2O molecules.[8] Since the organic linkers are hydrophobic in nature, the possible interaction sites for D_2O molecules is also expected to be near the C=O group. In addition, a new band of lower intensity at 1678 cm^{-1} appeared. This could be due to adjacent C=O bonds interacting with each other. Two new features at 1558 cm^{-1} and 1357 cm^{-1} also appeared, and this is due to perturbation of the $\nu_{asym}COO^-$ and $\nu_{sym}COO^-$ vibrational modes by D_2O molecules, respectively.[8] Negative peaks at 1234 cm^{-1}, 1051 cm^{-1} and 1016 cm^{-1} are also observed. For the activated Zn-DMOF-TM sample, these frequencies are assigned as the νCN and δCN vibrations.[7] These suggest that the C-N bonds are also perturbed by D_2O molecules. No bands were observed in the difference spectrum after the sample was evacuated and re-activated, indicating that D_2O vapor induces a reversible change.

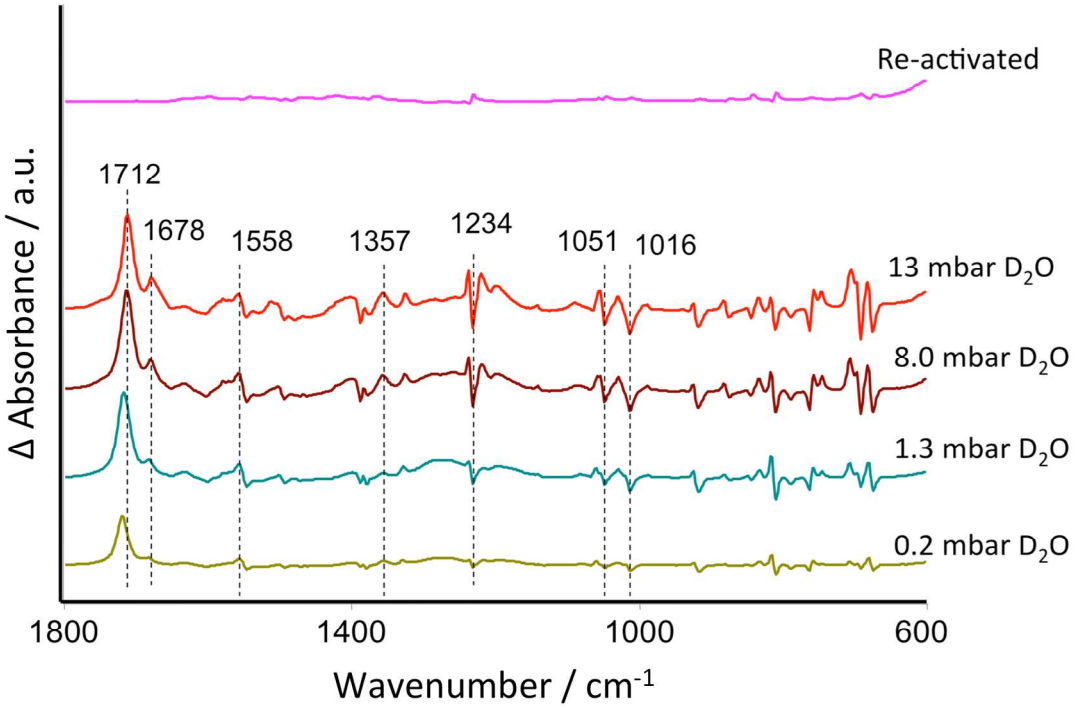

Figure S6. FTIR difference spectra of activated Zn-DMOF-TM exposed to various pressures of D_2O vapor followed by sample re-activation.

Simulation Section

All classical simulations were performed using the RASPA[9] simulation code with molecular dynamics simulations performed in the NVT ensemble. The quantum mechanical DABCO rotation energy profile at 0 K was obtained using the VASP code using projector-augmented wave method pseudopotentials[10] with the Perdew−Burke−Ernzerhof generalized- gradient approximation,[11] single k-point sampling, and 780 eV plane wave cut-offs.

Flexible Framework Parameters

Flexible framework models for the Zn-DMOF and Zn-DMOF-TM structures were adapted from previously developed models.[12,13] The main differences are a change from a GAFF type model for the ligand parameters to OPLS, and improved parameters for the Ca-Ca-C_2-Ox torsion. Also, VDW-interactions were evaluated using a cutoff at a shifted potential at 12 Å (i.e. no tail-corrections). The metal-parameters are based on the original Grosch and Paesani DMOF model.[13] In this work, the Zn-DMOF and Zn-DMOF-TM models were analyzed to ensure consistency between characteristics of the classical and *ab initio* energy profiles for the rotation of DABCO inside of the structure at 0 K.

Zn-DMOF Parameters

Bond	**type**	**k_0/k_B [K]**	**r_0 [Å]**	**k_1 [Å^{-1}]**
Zn-O_1	Morse	11946.93	2.169	1.4986
Zn-O_2	Morse	11946.93	2.169	1.4986
Zn-N_3	Morse	21939.86	2.04108	1.422750
Zn-Zn	Harmonic	69233.93	2.72914	
O_1-C_2	Harmonic	660223.85	1.25	
O_2-C_2	Harmonic	660223.85	1.25	
C_2-C_{a1}	Harmonic	472019.79	1.409	
C_{a1}-C_{a2}	Harmonic	472019.79	1.40	
C_{a2}-C_{a2}	Harmonic	472019.79	1.40	
C_{a2}-H_a	Harmonic	369363.04	1.08	
N_3-C_3	Harmonic	369363.04	1.471	
C_3-C_3	Harmonic	311996.02	1.526	
H_2-C_3	Harmonic	342189.19	1.09	

Table S1: Defined bond potentials for the flexible DMOF model. Two function forms are used: (1) the Morse potential $\boldsymbol{U = k_0\left[\left(1 - e^{-k_1(r-r_0)}\right)^2 - 1\right]}$, and (2) the harmonic bond potential $\boldsymbol{U = \frac{1}{2}k(r - r_0)^2}$. The nearest neighbor 1-2 interactions are omitted in the VDW and electrostatics terms.

Bend	type	k/k_B [K]	θ_0 [°]
O_1-Zn-O_2	Harmonic	17609.16	85.793
O_1-Zn-O_1	Harmonic	12724.41	168.517
O_2-Zn-O_2	Harmonic	12724.41	168.517
O_1-Zn-N_3	Harmonic	35593.21	92.275
O_2-Zn-N_3	Harmonic	35593.21	92.275
Zn-O_1-C_2	Harmonic	24313.05	158.423
Zn-O_2-C_2	Harmonic	24313.05	158.423
O_1-C_2-O_1	Harmonic	80515.10	140.0
O_2-C_2-O_2	Harmonic	80515.10	140.0
O_1-C_2-O_2	Harmonic	80515.10	140.0
O_1-C_2-C_{a1}	Harmonic	63405.64	120.0
O_2-C_2-C_{a1}	Harmonic	63405.64	120.0
C_2-C_{a1}-C_{a2}	Harmonic	63405.64	120.0
C_{a1}-C_{a2}-C_{a2}	Harmonic	63405.64	120.0
C_{a2}-C_{a1}-C_{a2}	Harmonic	63405.64	120.0
C_{a1}-C_{a2}-H_a	Harmonic	50321.94	120.0
C_{a2}-C_{a2}-H_a	Harmonic	50321.94	120.0
H_2-C_3-H_2	Harmonic	35225.36	109.0
C_3-C_3-H_2	Harmonic	50321.94	109.5
H_2-C_3-N_3	Harmonic	50321.94	109.5
C_3-C_3-N_3	Harmonic	80515.10	111.2
C_3-N_3-C_3	Harmonic	50321.94	109.5

Table S2: Defined bend potentials for the flexible DMOF model using the harmonic bend potential: $\boldsymbol{U = \frac{1}{2}k(\theta - \theta_0)^2}$. The nearest neighbor 1-3 interactions are omitted in the VDW and electrostatics terms. The O_X-Zn-O_X has two bend potential with different reference angles, which necessitates the use of two types of oxygen O_1 and O_2 (the type O_X refers to both).

Improper torsion	type	k_0/k_B [K]	k_1/k_B [K]	k_2/k_B [K]	k_3/k_B [K]
O_1-C_2-O_1-C_{a1}	opls	0	0	5283.80	0
O_1-C_2-O_2-C_{a1}	opls	0	0	5283.80	0
O_2-C_2-O_1-C_{a1}	opls	0	0	5283.80	0
O_2-C_2-O_2-C_{a1}	opls	0	0	5283.80	0
H_a-C_{a2}-C_{a2}-C_{a1}	opls	0	0	553.54	0
C_{a2}-C_{a1}-C_{a2}-C_2	opls	0	0	553.54	0

Table S3: Defined improper torsion potentials for the flexible DMOF model where the second atom is the central atom to which the other three are bonded. The functional form is the same as for the below torsions.

Torsion	type	k_1/k_B [K]	k_2/k_B [K]	k_3/k_B [K]	VDW Scaling	Electrostatic Scaling
Zn-N_3-C_3-H_2	opls	0	0	0	1/2	1/8
Zn-N_3-C_3-C_3	opls	0	0	0	1/2	1/8
O_1-Zn-N_3-C_3	opls	0	0	0	1/2	1/8
O_2-Zn-N_3-C_3	opls	0	0	0	1/2	1/8
Zn-Zn-N_3-C_3	opls	0	0	0	1/2	1/8
Zn-O_1-C_2-C_{a1}	opls	0	715.58	0	1/2	1/8
Zn-O_2-C_2-C_{a1}	opls	0	715.58	0	1/2	1/8
O_1-Zn-O_1-C_2	opls	0	0	0	1/2	1/8
O_2-Zn-O_2-C_2	opls	0	0	0	1/2	1/8
Zn-O_1-C_2-O_1	opls	0	712.06	0	1/2	1/8
Zn-O_2-C_2-O_2	opls	0	712.06	0	1/2	1/8
Zn-O_1-C_2-O_2	opls	0	712.06	0	1/2	1/8
Zn-O_2-C_2-O_1	opls	0	712.06	0	1/2	1/8
N_3-C_3-C_3-N_3	opls	0	0	78.50	1/2	1/8
N_3-C_3-C_3-H_2	opls	0	0	78.50	1/2	1/8
C_3-N_3-C_3-H_2	opls	0	0	150.97	1/2	1/8
C_3-C_3-N_3-C_3	opls	0	120.77	0	1/2	1/8
C_3-C_3-N_3-C_3	opls	0	0	75.48	1/2	1/8
H_2-C_3-C_3-H_2	opls	0	0	78.50	1/2	1/8
C_{a2}-C_{a1}-C_2-O_1	opls	0	1358.69	0	1/2	1/8
C_{a2}-C_{a1}-C_2-O_2	opls	0	1358.69	0	1/2	1/8
C_2-C_{a1}-C_{a2}-H_a	opls	0	1824.17	0	1/2	1/8
C_2-C_{a1}-C_{a2}-C_{a2}	opls	0	1824.17	0	1/2	1/8
C_{a1}-C_{a2}-C_a2-C_{a1}	opls	0	1824.17	0	1/2	1/8
C_{a1}-C_{a2}-C_{a2}-H_a	opls	0	1824.17	0	1/2	1/8
C_{a2}-C_{a1}-C_{a2}-C_{a2}	opls	0	1824.17	0	1/2	1/8
C_{a2}-C_{a1}-C_{a2}-H_a	opls	0	1824.17	0	1/2	1/8
H_a-C_{a2}-C_{a2}-H_a	opls	0	1824.17	0	1/2	1/8

Table S4: Defined torsion potentials for the flexible DMOF model using the using the OPLS functional: $\boldsymbol{U = 1/2k_1[1 + cos(\phi)] + 1/2k_2[1 - cos(2\phi)] + 1/2k_3[1 + cos(3\phi)]}$. The 1-4 long-range interactions are omitted unless defined via 1-4 torsion interactions. The VDW interaction and 1-4 charge-charge interactions of the torsions are scaled with the values listed in the final two columns.

Type	Potential-type	ε/k_B [K]	σ [Å]	q (e)
Zn	Lennard-Jones	6.290	2.4945	1.1832
O_1	Lennard-Jones	105.676	2.9599	-0.7372
O_2	Lennard-Jones	105.676	2.9599	-0.7372
C_2	Lennard-Jones	35.2254	3.55	0.7904
C_{a1}	Lennard-Jones	35.2254	3.55	-0.0503
C_{a2}	Lennard-Jones	35.2254	3.55	-0.0955
H_a	Lennard-Jones	15.0966	2.42	0.1018
H_2	Lennard-Jones	15.0966	2.50	0.0372
N_3	Lennard-Jones	85.5473	3.25	0.0415
C_3 (dabco)	Lennard-Jones	33.2125	3.50	-0.0015

Table S5: Defined van der Waals parameters for the flexible DMOF model using the function form: $\boldsymbol{U = 4\varepsilon\left[\left(\frac{\sigma}{r}\right)^{12} - \left(\frac{\sigma}{r}\right)^{6}\right]}$. Cutoff is 12 Å and the potential is shifted to zero at the cutoff.

Zn-DMOF-TM Parameters

Bond	type	k_0/k_B [K]	r_0 [Å]	k_1 [$Å^{-1}$]
Zn-O_1	Morse	11946.93	2.169	1.4986
Zn-O_2	Morse	11946.93	2.169	1.4986
Zn-N_3	Morse	21939.86	2.04108	1.422750
Zn-Zn	Harmonic	69233.93	2.72914	
O_1 -C_2	Harmonic	660223.85	1.25	
O_2 -C_2	Harmonic	660223.85	1.25	
C_2 -C_{a1}	Harmonic	472019.79	1.409	
C_{a1}-C_{a2}	Harmonic	472019.79	1.40	
C_{a2}-C_{a2}	Harmonic	472019.79	1.40	
N_3-C_3	Harmonic	369363.04	1.471	
C_3-C_3	Harmonic	311996.02	1.526	
H_2-C_3	Harmonic	342189.19	1.09	
C_m-H_m	Harmonic	342189.19	1.09	
C_{a2}-C_m	Harmonic	319041.10	1.51	

Table S6: Defined bond potentials for the flexible DMOF-TM model. Two function forms are used: (1) the Morse potential $\boldsymbol{U = k_0\left[\left(1 - e^{-k_1(r-r_0)}\right)^2 - 1\right]}$, and (2) the harmonic bond potential $\boldsymbol{U = \frac{1}{2}k(r - r_0)^2}$. The nearest neighbor 1-2 interactions are omitted in the VDW and electrostatics terms.

Bend	type	k/k_B [K]	θ_0 [°]
O_1-Zn-O_2	Harmonic	17609.16	85.793
O_1-Zn-O_1	Harmonic	12724.41	168.517
O_2-Zn-O_2	Harmonic	12724.41	168.517
O_1-Zn-N_3	Harmonic	35593.21	92.275
O_2-Zn-N_3	Harmonic	35593.21	92.275
Zn-O_1-C_2	Harmonic	24313.05	158.423
Zn-O_2-C_2	Harmonic	24313.05	158.423
O_1-C_2-O_1	Harmonic	80515.10	140.0
O_2-C_2-O_2	Harmonic	80515.10	140.0
O_1-C_2-O_2	Harmonic	80515.10	140.0
O_1-C_2-C_{a1}	Harmonic	63405.64	120.0
O_2-C_2-C_{a1}	Harmonic	63405.64	120.0
C_2-C_{a1}-C_{a2}	Harmonic	63405.64	120.0
C_{a1}-C_{a2}-C_{a2}	Harmonic	63405.64	120.0
C_{a2}-C_{a1}-C_{a2}	Harmonic	63405.64	120.0
H_2-C_3-H_2	Harmonic	35225.36	109.0
C_3-C_3-H_2	Harmonic	50321.94	109.5
H_2-C_3-N_3	Harmonic	50321.94	109.5
C_3-C_3-N_3	Harmonic	80515.10	111.2
C_3-N_3-C_3	Harmonic	50321.94	109.5
C_{a1}-C_{a2}-C_m	Harmonic	70450.74	120.0
C_{a2}-C_{a2}-C_m	Harmonic	70450.74	120.0
C_{a2}-C_m-H_m	Harmonic	50321.96	109.5
H_m-C_m-H_m	Harmonic	35225.37	109.5

Table S7: Defined bend potentials for the flexible DMOF-TM model using the harmonic bend potential: $\boldsymbol{U = \frac{1}{2}k(\theta - \theta_0)^2}$. The nearest neighbor 1-3 interactions are omitted in the VDW and electrostatics terms. The O_X-Zn-O_X has two bend potential with different reference angles, which necessitates the use of two types of oxygen O_1 and O_2 (the type O_X refers to both).

Improper torsion	type	k_0/k_B [K]	k_1/k_B [K]	k_2/k_B [K]	k_3/k_B [K]
O_1-C_2-O_1-C_{a1}	opls	0	0	5283.80	0
O_1-C_2-O_2-C_{a1}	opls	0	0	5283.80	0
O_2-C_2-O_1-C_{a1}	opls	0	0	5283.80	0
O_2-C_2-O_2-C_{a1}	opls	0	0	5283.80	0
C_{a2}-C_{a1}-C_{a2}-C_2	opls	0	0	553.54	0
C_{a1}-C_{a2}-C_{a2}-C_m	opls	0	0	553.54	0

Table S8: Defined improper torsion potentials for the flexible DMOF-TM model where the second atom is the central atom to which the other three are bonded. The functional form is the same as for the below torsions.

Torsion	type	k_1/k_B [K]	k_2/k_B [K]	k_3/k_B [K]	VDW Scaling	Electrostatic Scaling
Zn-N_3-C_3-H_2	opls	0	0	0	1/2	1/8
Zn-N_3-C_3-C_3	opls	0	0	0	1/2	1/8
O_1-Zn-N_3-C_3	opls	0	0	0	1/2	1/8
O_2-Zn-N_3-C_3	opls	0	0	0	1/2	1/8
Zn-Zn-N_3-C_3	opls	0	0	0	1/2	1/8
Zn-O_1-C_2-C_{a1}	opls	0	715.58	0	1/2	1/8
Zn-O_2-C_2-C_{a1}	opls	0	715.58	0	1/2	1/8
O_1-Zn-O_1-C_2	opls	0	0	0	1/2	1/8
O_2-Zn-O_2-C_2	opls	0	0	0	1/2	1/8
Zn-O_1-C_2-O_1	opls	0	712.06	0	1/2	1/8
Zn-O_2-C_2-O_2	opls	0	712.06	0	1/2	1/8
Zn-O_1-C_2-O_2	opls	0	712.06	0	1/2	1/8
Zn-O_2-C_2-O_1	opls	0	712.06	0	1/2	1/8
N_3-C_3-C_3-N_3	opls	0	0	78.50	1/2	1/8
N_3-C_3-C_3-H_2	opls	0	0	78.50	1/2	1/8
C_3-N_3-C_3-H_2	opls	0	0	150.97	1/2	1/8
C_3-C_3-N_3-C_3	opls	0	120.77	0	1/2	1/8
C_3-C_3-N_3-C_3	opls	0	0	75.48	1/2	1/8
H_2-C_3-C_3-H_2	opls	0	0	78.50	1/2	1/8
C_{a2}-C_{a1}-C2-O_1	opls	0	1157.40	0	1/2	1/8
C_{a2}-C_{a1}-C2-O_2	opls	0	1157.40	0	1/2	1/8
C_2-C_{a1}-C_{a2}-C_m	opls	0	1824.17	0	1/2	1/8
C_2-C_{a1}-C_{a2}-C_{a2}	opls	0	1824.17	0	1/2	1/8
C_{a1}-C_{a2}-C_{a2}-C_{a1}	opls	0	1824.17	0	1/2	1/8
C_{a1}-C_{a2}-C_{a2}-C_m	opls	0	1824.17	0	1/2	1/8
C_{a2}-C_{a1}-C_{a2}-C_{a2}	opls	0	1824.17	0	1/2	1/8
C_{a2}-C_{a1}-C_{a2}-C_m	opls	0	1824.17	0	1/2	1/8
C_m-C_{a2}-C_{a2}-C_m	opls	0	1824.17	0	1/2	1/8
C_{a2}-C_{a2}-C_m-H_m	opls	-218.90	0	-42.77	1/2	1/8
C_{a1}-C_{a2}-C_m- H_m	opls	-218.90	0	-42.77	1/2	1/8

Table S9: Defined torsion potentials for the flexible DMOF-TM model using the using the OPLS functional: $\boldsymbol{U = 1/2k_1[1 + cos(\phi)] + 1/2k_2[1 - cos(2\phi)] + 1/2k_3[1 + cos(3\phi)]}$. The 1-4 long-range interactions are omitted unless defined via 1-4 torsion interactions. The VDW interaction and 1-4 charge-charge interactions of the torsions are scaled with the values listed in the final two columns.

Type	Potential-type	ε/k_B [K]	σ [Å]	q (e)
Zn	Lennard-Jones	6.290	2.4945	1.1832
O_1	Lennard-Jones	105.676	2.9599	-0.7372
O_2	Lennard-Jones	105.676	2.9599	-0.7372
C_2	Lennard-Jones	35.2254	3.55	0.7904
C_{a1}	Lennard-Jones	35.2254	3.55	-0.0503
C_{a2}	Lennard-Jones	35.2254	3.55	0.0063
H_2	Lennard-Jones	15.0966	2.50	0.0372
N_3	Lennard-Jones	85.5473	3.25	0.0415
C_3 (dabco)	Lennard-Jones	33.2125	3.50	-0.0015
H_m (methyl)	Lennard-Jones	15.0966	2.50	0.074
C_m (methyl)	Lennard-Jones	33.2125	3.50	-0.222

Table S10: Defined van der Waals parameters for the flexible DMOF-TM model using the function form: $\boldsymbol{U = 4\varepsilon\left[\left(\frac{\sigma}{r}\right)^{12} - \left(\frac{\sigma}{r}\right)^{6}\right]}$. Cutoff is 12 Å and the potential is shifted to zero at the cutoff.

DABCO 0 K Rotation Energy Profiles

Figure S8 and S9 compare the energy barrier obtained from single point calculations for rotating a single DABCO around its N-N axis in the Zn-DMOF and Zn-DMOF-TM structures at 0 K using the classical flexible framework models versus quantum mechanical calculations with the van der Waals interactions correction method of Grimme.[14] While the quantum mechanical barrier exceeds that of the classical models by ~ 3-4 kJ/mol, both profiles capture the same characteristic features and are low in energy compared to interaction energies introduced by water. Isolation of the contributions to the energy profile obtained from the classical models due to coulombic interactions indicates that it is the van der Waals contributions that play the most significant role and, furthermore, the removal of all van der Waals interactions except those between DABCO and the carboxylate oxygen atoms in the framework indicates that it is the these particular van der Waals interactions that govern the energy profiles in both structures (figures S10 and S11). The relatively small difference in energetics observed when removing the van der Waals interactions correction method of Grimme[14] from the quantum mechanical calculations (figures S12 and S13) also indicates that these rotation energies are governed primarily by short-range, repulsive van der Waals forces.

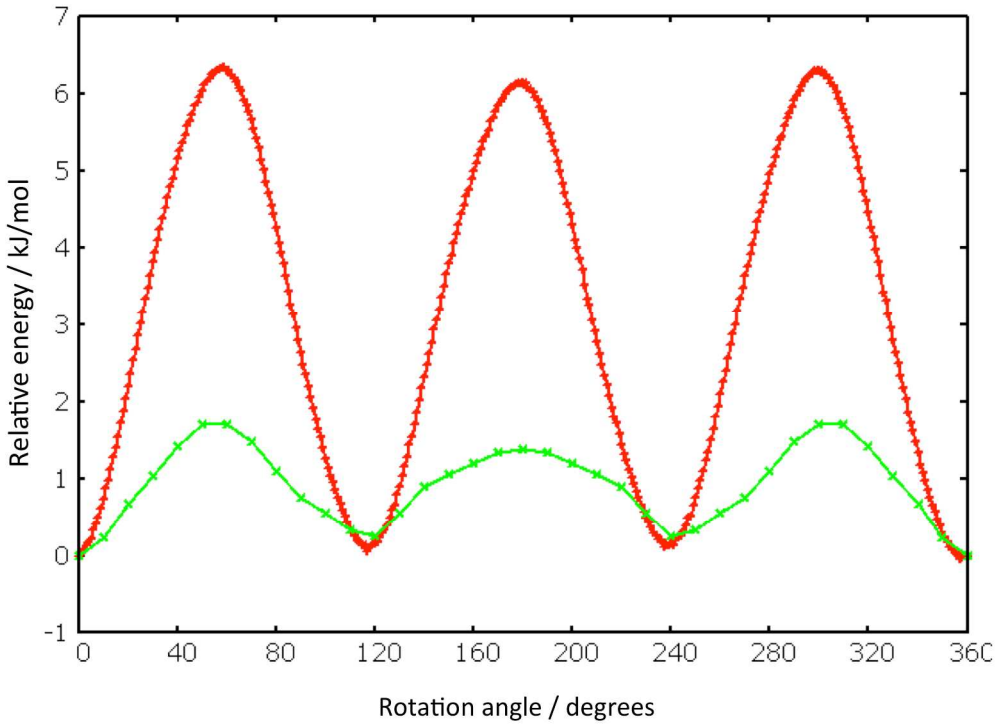

Figure S7. Profile showing the change in energy for rotating a single DABCO around its N-N axis in the Zn-DMOF structure at 0 K using the classical flexible framework model (green) versus in the Zn-DMOF structure using quantum mechanical calculations (red) with the van der Waals interactions correction method of Grimme.[14]

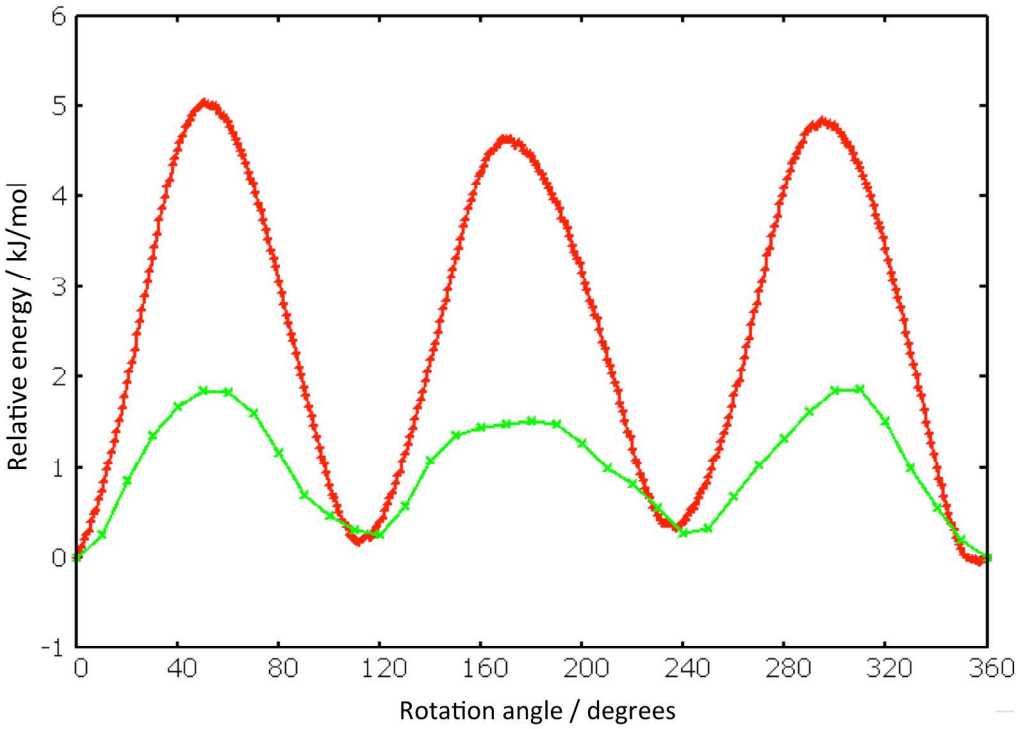

Figure S8. Profile showing the change in energy for rotating a single DABCO around its N-N axis in the Zn-DMOF-TM structure at 0 K using the classical flexible framework model (green) versus in the Zn-DMOF-TM structure using quantum mechanical calculations (red) with the van der Waals interactions correction method of Grimme.[14]

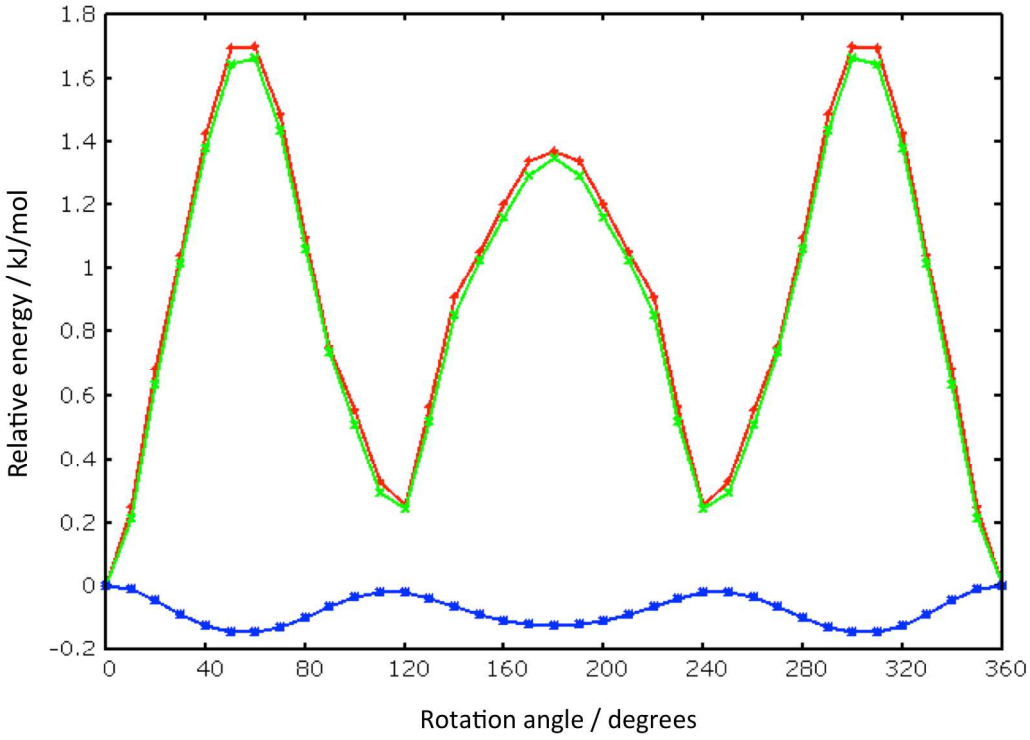

Figure S9. Profile showing the change in energy for rotating a single DABCO around its N-N axis in the Zn-DMOF structure obtained from the classical model results (red). Contributions to the total energy due to coulombic contributions are shown in blue. The green curve shows the energy profile with all van der Waals interactions removed except for those between DABCO and the carboxylate oxygen atoms in the framework.

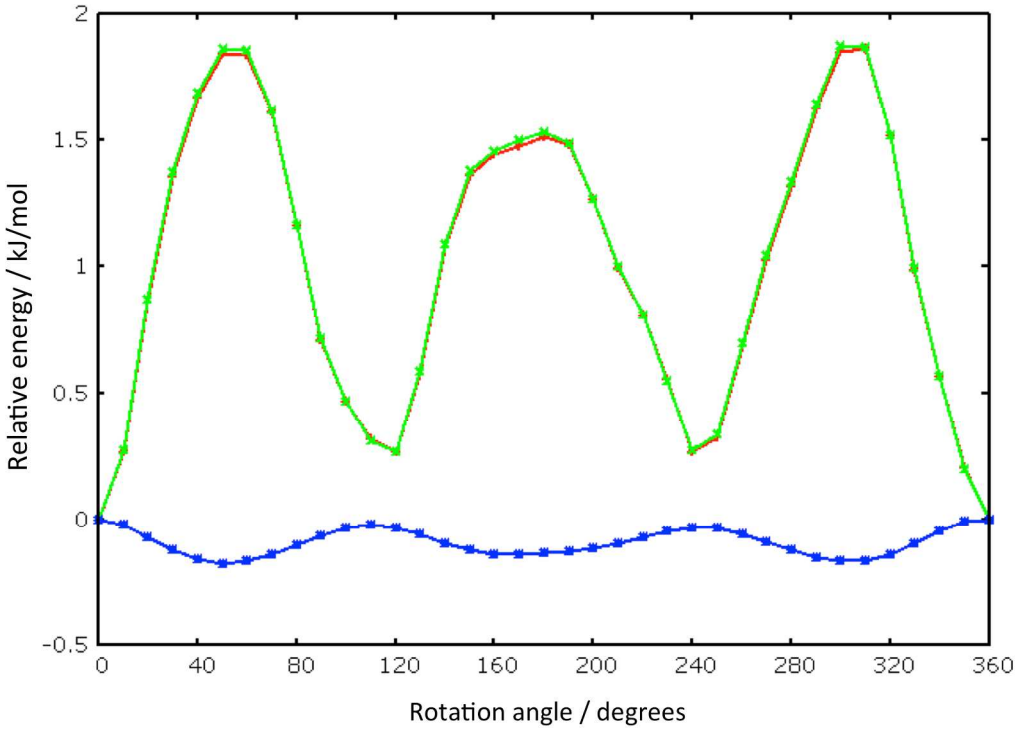

Figure S10. Profile showing the change in energy for rotating a single DABCO around its N-N axis in the Zn-DMOF-TM structure obtained from the classical model results (red). Contributions to the total energy due to coulombic contributions are shown in blue. The green curve shows the energy profile with all van der Waals interactions removed except for those between DABCO and the carboxylate oxygen atoms in the framework.

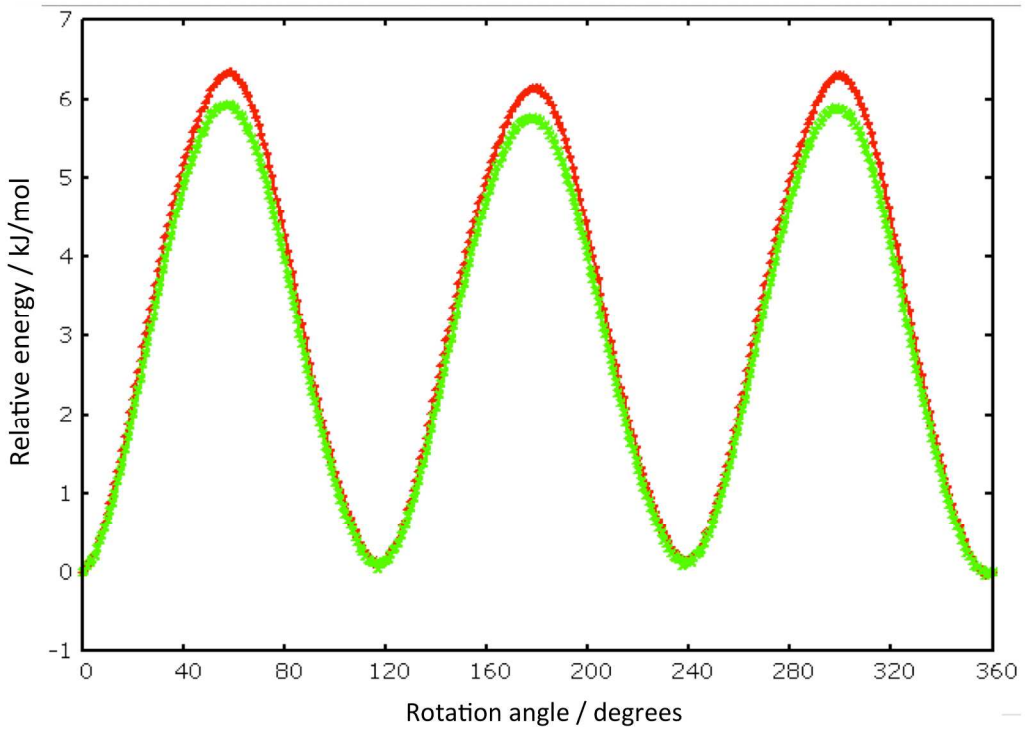

Figure S11. Profile showing the change in energy for rotating a single DABCO around its N-N axis in the Zn-DMOF structure at 0 K using quantum mechanical calculations with (red) and without (green) the van der Waals interactions correction method of Grimme.[14]

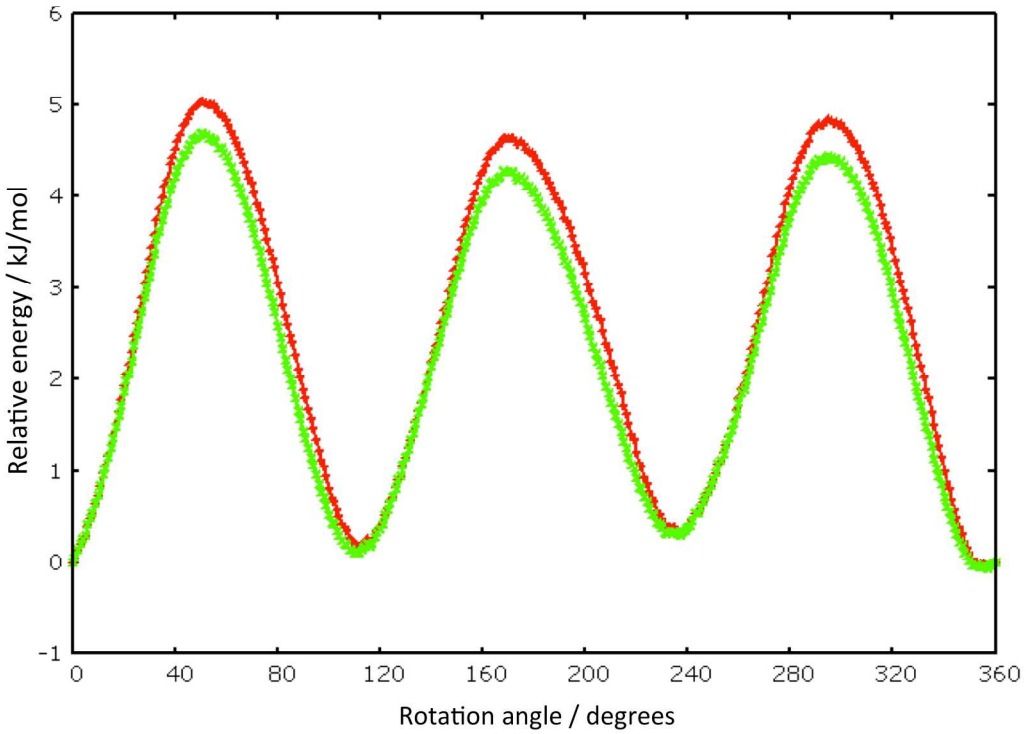

Figure S12. Profile showing the change in energy for rotating a single DABCO around its N-N axis in the Zn-DMOF-TM structure at 0 K using quantum mechanical calculations with (red) and without (green) the van der Waals interactions correction method of Grimme.[14]

References

1. Jasuja, H.; Burtch, N. C.; Huang, Y.-G.; Cai, Y.; Walton, K. S., Kinetic water stability of an isostructural family of zinc-based pillared metal-organic frameworks. *Langmuir* **2013,** 29, (2).
2. Walton, K. S.; Snurr, R. Q., Applicability of the BET method for determining surface areas of microporous metal-organic frameworks. *Journal of the American Chemical Society* **2007,** 129, (27).
3. Dueren, T.; Millange, F.; Ferey, G.; Walton, K. S.; Snurr, R. Q., Calculating geometric surface areas as a characterization tool for metal-organic frameworks. *Journal of Physical Chemistry C* **2007,** 111, (42).
4. Schmidt-Rohr, K.; Clauss, J.; Spiess, H. W., Correlation of structure, mobility, and morphological information in heterogenous polymer materials by 2-dimensional wideline-separation NMR-spectroscopy. *Macromolecules* **1992,** 25, (12).
5. Dixon, W. T., Spinning-Sideband-Free NMR-Spectra. *Journal of Magnetic Resonance* **1981,** 44, (1).
6. Spiess, H. W., Molecular-dynamics of solid polymers as revealed by deuteron NMR. *Colloid and Polymer Science* **1983,** 261, (3).
7. Socrates, G., *Infrared and Raman Characteristic Group Frequencies*. Third ed.; John Wiley & Sons LTD: 2001; p 343.
8. Tan, K.; Nijem, N.; Canepa, P.; Gong, Q.; Li, J.; Thonhauser, T.; Chabal, Y. J., Stability and Hydrolyzation of Metal Organic Frameworks with Paddle-Wheel SBUs upon Hydration. *Chemistry of Materials* **2012,** 24.
9. Dubbeldam, D.; Calero, S.; Ellis, D.E.; Snurr, R.Q. RASPA: Molecular Simulation Software for Adsorption and Diffusion in Flexible Nanoporous Materials. *Molecular Simulation* **2015** (DOI: 10.1080/08927022.2015.1010082)
10. Blochl, P. E., Projector Augmented-Wave Method. *Physical Review B* **1994,** 50, (24).
11. Perdew, J. P.; Burke, K.; Ernzerhof, M., Generalized gradient approximation made simple. *Physical Review Letters* **1996,** 77.
12. Burtch, N. C.; Jasuja, H.; Dubbeldam, D.; Walton, K. S., Molecular-level Insight into Unusual Low Pressure CO2 Affinity in Pillared Metal-Organic Frameworks. *Journal of the American Chemical Society* **2013,** 135, (19).
13. Grosch, J. S.; Paesani, F., Molecular-Level Characterization of the Breathing Behavior of the Jungle-Gym-type DMOF-1 Metal-Organic Framework. *Journal of the American Chemical Society* **2012,** 134, (9).
14. Grimme, S., Semiempirical GGA-type density functional constructed with a long-range dispersion correction. *Journal of Computational Chemistry* **2006,** 27, (15).